Defects and magnetic hyperfine fields in $ZrFe_2$ investigated using perturbed-angular-correlation spectroscopy

Arthur T. Motta, Gary L. Catchen, and Stephen E. Cumblidge
Department of Mechanical and Nuclear Engineering, The Pennsylvania State University, University Park, Pennsylvania 16802

R. L. Rasera
Department of Physics, University of Maryland, Baltimore, Maryland 21250

Andrea Paesano, Jr.
Universidade Estadual de Maringá, Maringá, Paraná, Brazil

Livio Amaral
Instituto de Fisica, Universidade Federal do Rio Grande do Sul, Porto Alegre, Rio Grande do Sul, Brazil
(Received 20 August 1998; revised manuscript received 31 December 1998)

We have measured the temperature dependence of the electric and magnetic hyperfine interactions at ^{181}Ta nuclei substituted into the Zr site in the Laves-phase compound $ZrFe_2$, using the perturbed angular correlation of γ rays emitted after the β^- decays of ^{181}Hf probe nuclei. Although the overall crystal structure is cubic, a weak strongly damped electric-quadrupole interaction is observed, which shows no significant temperature dependence over the investigated temperature range from 290–1300 K. Thus below the magnetic ordering temperature T_C of 631(2) K we observe combined magnetic-dipole and electric-quadrupole hyperfine interactions. Two separate magnetic components characterize the magnetic-dipole interactions. For the interaction at the primary site, which is occupied by 70–80% of the probes, the Larmor frequency measured at temperature has a value of $\omega_L = 407(1)$ Mrad sec^{-1}. The secondary site is populated by the remaining 20–30% of the probes, for which the corresponding Larmor frequency has a room temperature value of $\omega_L = 579(3)$ Mrad sec^{-1}. We attribute the primary interaction to the ''perfect-crystal'' probe environment at the Zr site, whereas we ascribe the secondary interaction to the enhancement of the transferred hyperfine field by the presence of Fe antisite defects near the Zr site. At temperatures below but very close to T_C, those frequencies cannot be determined for either interaction, because the magnetic-hyperfine and the electric-quadrupole frequencies converge to comparable values. [S0163-1829(99)06025-7]

I. INTRODUCTION

Intermetallic compounds, such as the Laves-phase $ZrFe_2$, differ fundamentally from ordinary alloys of metals, because the constituent metal atoms exhibit long-range structural order in the crystal. Binary intermetallic compounds consist therefore of crystals that have two distinct sublattices. If one or both constituent atoms have either *d* or *f* electrons that can order via the exchange interaction, then both structural and magnetic ordering characterize the intermetallic crystal. Defects, dopants, and impurities affect the properties of intermetallic compound by breaking the symmetry of the crystal structure. This reduction in symmetry may affect only the local environment of a defect; or, alternatively, this reduction may modify the long-range magnetic ordering in the crystal. The fundamental purpose of this investigation therefore is to understand the effects of defects and magnetism that take place on a nanometer scale in the context of the macroscopic structural and magnetic properties of the crystal.

For this purpose, we use perturbed-angular-correlation (PAC) spectroscopy,[1] because with it we can observe local structural changes that point defects produce via the nuclear electric-quadrupole interaction and concurrently the long-range effects that magnetic ordering produce via the nuclear magnetic-dipole interaction. The PAC technique is based on substituting a relatively low concentration of a radioactive probe atom, in this case, $^{181}\text{Hf}\rightarrow{}^{181}\text{Ta}$, into a well-defined site in a crystal. Because the chemistries of Hf and Zr are very similar, the probe $^{181}\text{Hf}\rightarrow{}^{181}\text{Ta}$ substitutes into the Zr site in $ZrFe_2$. This probe can be added at relatively low levels, $\leqslant 0.1$ at. % Hf, so that it does not measurably alter the global properties of the crystal. Because of this sensitivity, PAC spectroscopy provides a unique means to investigate the nanometer-scale effects of local crystal and magnetic fields at the Zr site in $ZrFe_2$. At the probe site, the former generate electric-field gradients (EFG's), when the site symmetry is lower than cubic; and the latter generate magnetic hyperfine fields (MHF's), which can be measured below the magnetic ordering temperature T_C (i.e., the Curie temperature). Specifically, we measured EFG's and MHF's in the compounds $(Zr_{1-x},Hf_x)\,Fe_{2+y}$, temperatures ranging from 290–1300 K, for values of *x* varying from 0.003–0.05, and for values of *y* varying from 0–0.1. Experiments were repeated several times, and were performed while both increasing and decreasing the temperature.

The compound $ZrFe_2$ crystallizes in the C15 $MgCu_2$-type Laves-phase structure.[2,3] The stoichiometry corresponding to the C15 structure ranges approximately from 66–72 at. % Fe.[4] Thus we can take advantage of the range of composition over which the C15 structure is stable. By increasing the Fe concentration to slightly greater than 66 at. %, we can cause

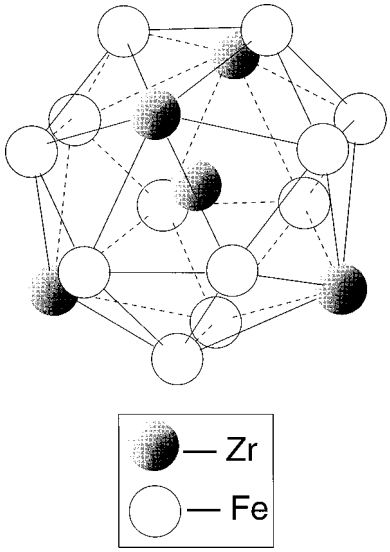

FIG. 1. Diagram of the nearest-neighbor environment of the Zr site in the C15 $MgCu_2$-type Laves-phase structure for $ZrFe_2$. The first-nearest neighbors are 4 Zr atoms and 12 Fe.

the formation of Fe antisite defects (Fe atoms that reside on Zr sites).

Because the local symmetry at the Fe site is lower than cubic, EFG's are present at the Fe site. When the crystal orders magnetically, the Fe sites, which are crystallographically equivalent above the magnetic ordering temperature, separate into two magnetically nonequivalent Fe sites, which have a population ratio of 3–1.[5,6] However, the PAC technique probes only the sites where the probes are. Figure 1 presents a schematic diagram of the nearest-neighbor environment of a Zr site, where the Hf probes are located. Four Zr atoms and 12 Fe atoms are located in the nearest-neighbor environment of the Zr site. The crystal contains only one crystallographic site for Zr, and the local symmetry at the Zr site is cubic. Based on this information, for Hf probes at the Zr site, we would expect to observe no EFG's and one single well-defined magnetic-dipole interaction below T_C, and a nonperturbed correlation above T_C.

However, earlier measurements on this compound (reviewed below) using a variety of techniques, indicate that these expectations do not correspond to reality. Instead, weak EFG's and two well-defined MHF's characterize hyperfine interactions at the Zr site in $ZrFe_2$. These measurements provide little detailed information about the origins of the unexpected weak EFG's and the nature of these MHF's. Therefore we have investigated in detail the magnetic-ordering phase transition by measuring the dependence of the MHF's temperatures up to T_C. In this context, we have determined that the primary MHF arises from a ''perfect-crystal'' surrounding coordination of Fe and Zr atoms and the secondary MHF arises from a local environment that contains an antisite defect. The reproducibility and consistency of measurements performed on a variety of samples suggests strongly that the thermodynamically stable crystal structure crystallizes with a small amount of disorder.

II. EARLIER RELATED INVESTIGATIONS

The history of measuring hyperfine interactions and related quantities in this Laves phase is long. For this reason, we briefly mention the earlier investigations related to this work. Piegger and Craig[7] used magnetization measurements to determine that the magnetic moment at the Fe site in $ZrFe_2$ is $1.62\mu_B$ and that $ZrFe_2$ is ferromagnetic below 628 K. They note that the magnetic moment in the $ZrFe_2$ is reduced from the corresponding value of $2.2\mu_B$ observed in pure Fe. To explain this difference, they state that the Zr atoms donate electrons to the Fe atoms, creating a more nearly filled *d* shell in the compound.

In the initial measurements of Fe site hyperfine interactions using ^{57}Fe-Mössbauer-effect spectroscopy, Wertheim, Jaccarino, and Wernick[5] observed two combined electric-quadrupole and magnetic-dipole interactions below a magnetic ordering temperature $T_C = 586$ K, in the proportion 3:1. In $ZrFe_2$ the direction of easy magnetization is $\langle 111 \rangle$. When the sample is magnetized, at one of the sites, the direction of the EFG is aligned with this direction of easy magnetization; but, at the other site, the direction of the EFG lies at an angle of 70.3° to the direction of easy magnetization. Thus the two different interactions arise because the Fe atoms occupy crystallographically identical but magnetically different sites. Amaral, Livi, and Gomes[6] confirmed this interpretation.

Bruckner, Kleinstuck, and Schulze[8] investigated the dependence of the lattice parameter on deviations from stoichiometry. They found that the lattice parameter does not change for Fe compositions slightly below 66 at. % but that it decreases for Fe compositions between 66 and 72 at. %. According to the authors, this effect arises because crystals having excess Zr are not stable and because excess Fe can be accommodated in the structure up to 72 at. %. To determine how this Fe excess is accommodated in the structure, the authors exclude the possibility that Fe atoms could fit into interstitial sites by noting that the space filling in this structure is 71 at. %. So no interstitial sites are available in the structure that have a size comparable to that of an Fe atom. They analyzed their diffraction data using a least-squares fitting method, and found that the best fit was obtained by assuming that the departure from stoichiometry was accommodated by Fe antisite defects in the Zr sites (rather than vacancies or Fe tetrahedra in Zr sites).

Based on observations of a low value of the electronic specific-heat coefficient γ and small high-field susceptibility $\chi_{\rm hf}$, Muraoka, Shiga, and Nakamura[9] give strong evidence for ferromagnetism in $ZrFe_2$. They also note that excess Fe atoms increase the Curie temperature T_C and magnetization, because, when those atoms are accommodated as antisite defects, they are surrounded by other Fe atoms as nearest neighbors. This configuration creates a more stable local magnetic moment. They report $T_C = 630$ K and that the direction of easy magnetization is $\langle 111 \rangle$, which changes to $\langle 100 \rangle$ when 20 at. % Co is substituted for Fe. These authors and others[10] report that it is very difficult to make $ZrFe_2$ without some amount of antisite defects.

Livi, Amaral, and Fries[11] measured the dependence of the Zr-site MHF on Hf concentration in $(Zr_{1-x}Hf_x)Fe_2$ for $x = 0.01$, 0.03, 0.1, and 0.25 using PAC spectroscopy. Although Hf is very similar chemically to Zr and should substitute exclusively onto the Zr site, Livi, Amaral, and Fries measured two magnetic hyperfine fields, with values of 62.5 and 92 kOe at laboratory temperature, for the composition $x = 0.01$. They attributed the lower value to Hf atoms on Zr

sites in a perfect-crystal environment and the higher value to Hf atoms on Zr sites, where another Hf atom is located in one of the nearest-neighbor Zr sites. They also found that increasing the Hf concentration decreased the magnitude of the Zr-site hyperfine fields. Wiesinger and co-workers[10,12] used Mössbauer-effect and nuclear-magnetic-resonance (NMR) spectroscopies to investigate the magnetic properties of $Zr(Fe_{1-x}Co_x)_2$. Although their Mössbauer-effect results agree generally with those of Wertheim, Jaccarino, and Wernick,[5] they found additional features in the Mössbauer-effect spectra measured on the stoichiometric $ZrFe_2$ compound. They could only accurately fit the Mössbauer spectra by assuming an additional Fe spectrum, which corresponds to a direction of easy magnetization along ⟨110⟩. Thus their model includes two interactions, one corresponding to magnetization along ⟨111⟩ and one along ⟨110⟩. The authors associate the magnetization along ⟨110⟩ to the presence of Fe antisite defects on Zr sites. Their NMR measurements of the hyperfine field of the ^{91}Zr in $ZrFe_2$ agree with the results of Betsuyaki and Komura,[13] who report a hyperfine field of 135 kOe. They noted that the line shapes of the zero-field spin-echo spectra of ^{91}Zr are asymmetric, an unusual occurrence in a crystal site with cubic symmetry.

Mohn and Schwarz[14] have recently performed self-consistent spin-polarized energy-band calculations for $ZrFe_2$, which predict that a small *negative* magnetic moment of $-0.56\mu_B$ resides at the Zr site. Their calculations show a magnetic moment of $1.90\mu_B$ for the Fe atoms, resulting in a net moment of $1.62\mu_B$ per Fe atom, once the contribution from the Zr is deducted. According to these calculations, $ZrFe_2$ should be considered as a *ferrimagnetic* rather than *ferromagnetic* compound. The pressure dependence of the magnetization of $ZrFe_2$ measured by Dumelow *et al.*[15] and Armitage *et al.*[16] provide support for this interpretation.

Luck and Wang[17] recently performed heat-capacity measurements on $ZrFe_2$ using differential scanning calorimetry. They found a discontinuity in the heat-capacity curve at 586 K, which they ascribe to the critical temperature for magnetic ordering. They determined that $T_C = 586$ K, in agreement with the measurements of Wertheim, Jaccarino, and Wernick[5] and Komura and Shikazono[18] but in disagreement with the measurements of most other researchers noted above. Arias and Abriata[3] suggest that Komura and Shikazono may have obtained this last result because they used a $ZrFe_2$ sample that contained excess Fe.

In summary, a variety of spectroscopic and macroscopic techniques have been used to investigate the magnetic properties of $ZrFe_2$ in contexts that involve the effects of defects and dopants. For the most part, these reports do not present clear connections between magnetic effects and effects of defects. We present results that give a clear connection between measured MHF's and a prevalent defect type in $ZrFe_2$, namely, Fe antisite defects.

III. EXPERIMENTAL TECHNIQUES

Intermetallic alloys were prepared by arc melting the pure constituents within an Ar atmosphere. The purity of the starting materials was 99.8% Zr, 99.995% Fe, and 97% Hf (most of the impurity content in Zr is Hf and vice versa). Before melting, a Hf wire was irradiated with thermal neutrons in the Penn State Breazeale Reactor to produce the ^{181}Hf radioactivity via the ^{180}Hf(n,γ) nuclear reaction. The Zr and Hf pieces (containing radioactive ^{181}Hf and stable carrier ^{180}Hf) were first melted together to help ensure a homogeneous Zr-Hf solid solution, and then the Zr and Hf pieces were mixed with Fe to produce buttons of $(Zr_{1-x}, Hf_x)\ Fe_{2+y}$. Samples were usually melted three times, turning the sample after each melting to help achieve homogeneity. We measured the weight of the samples before and after melting and found negligible mass loss. Visual inspection of the samples indicated that the samples had a bright, shiny appearance. This observation strongly suggests that significant amounts of oxygen were not incorporated into the bulk samples during melting. This observation is supported by previous studies using Mössbauer effect techniques, and which did not detect any evidence of oxygen contamination in similar samples.[6] To form the $ZrFe_2$ phase requires no special heat treatment after melting. The x-ray-diffraction patterns measured on the as-melted radioactive $ZrFe_2$ samples could be indexed in accord with the C15 Laves-phase structure and indicated phase purity to within a few percent. For the PAC measurements samples were sealed under Ar in a fused-silica tube prior to measurement.

The PAC spectrometers[1] used in this study are equipped with four (BaF or CsF) scintillation detectors that give a nominal time resolution of 0.8–1.0 nsec full width at half maximum for the gamma rays emitted in the decays of ^{181}Hf. On one of the spectrometers we have designed and built a furnace and a very-high-precision temperature-control system, which can maintain a sample temperature to within ± 0.03 K at the set point for a measurement period of up to 24 h. This apparatus gives us the capability to investigate magnetic ordering phase transitions at temperatures very close to T_C.

For a polycrystalline sample and for the spin $I = \frac{5}{2}$ intermediate level of ^{181}Ta, the measured angular correlation function is given by[19]

$$W(\theta,t) \cong \exp(-t/\tau_N)[1 + A_{22}G_{22}(t)P_2(\cos\theta)], \quad (1)$$

where θ and t are the angle between emission directions of the cascade γ rays, and the time between emission of the first and second γ rays, respectively. τ_N represents the lifetime of the intermediate level of the ^{181}Ta probe nucleus, and A_{22} represents the corresponding anisotropy of the angular correlation. The perturbation function,

$$G_{22}(t) = S_0 + \sum_i S_i \cos(\omega_i)\exp(-\delta\omega_i t), \quad (2)$$

represents the extranuclear hyperfine interaction, where the parameter δ is a measure of the width of the Lorentzian distribution of the hyperfine frequencies about their mean values. The frequencies ω_i and their amplitudes S_i are related to the hyperfine splitting of the intermediate nuclear level. Above T_C where no MHF is present, three interaction frequencies ω_i are observable, related to the nuclear electric-quadrupole interaction (NQI) frequency $\omega_Q = eQV_{zz}/4I(2I-1)\hbar$ and the asymmetry parameter $\eta = (V_{xx} - V_{yy})/V_{zz}$, where the V_{ii} are the elements of the EFG tensor in its principal axis system. Below T_C, the frequencies ω_i are obtained by diagonalizing the hyperfine interaction matrix resulting

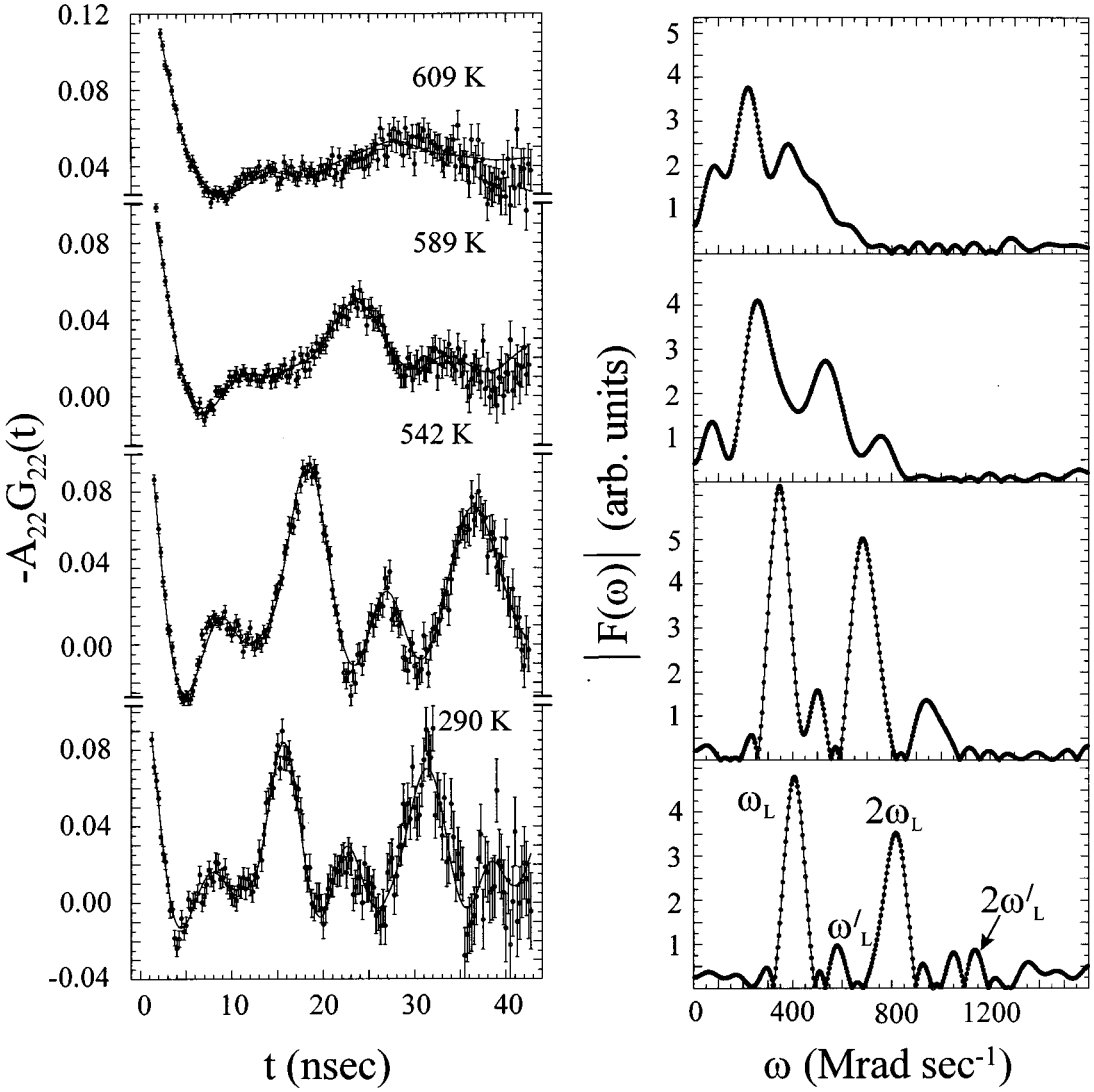

FIG. 2. Perturbation functions and corresponding Fourier transforms measured on a stoichiometric sample of $ZrFe_2$. The 290-K perturbation function and transform show relatively sharp lines, which are broadened by the effects of a weak poorly defined NQI. The fits represent a model of a combined magnetic-dipole and electric-quadrupole interaction, in which a NQI represents a perturbation to two strong magnetic-dipole interactions. At higher temperatures, the interaction frequencies become lower. The associated merging of the peaks in the transforms illustrates the difficulties that arise in the analysis of the corresponding perturbation functions.

from the combination of the NQI with the MHF represented by the magnetic frequency $\omega_L = -g_I \mu_N B/\hbar$, in which B represents the MHF, g_I represents the nuclear g factor [$g_I = 1.30(3)$], and μ_N represents the nuclear magneton. Because of the lifting of the degeneracy of the NQI by the addition of the MHF, the number of allowable ω_i is increased from 3 to (in principle) 15.[1] The hyperfine parameters were extracted from the measured perturbation functions $A_{22}G_{22}(t)$ using the DEPACK program developed by Lindgren.[20]

In the present set of experiments, we consider two distinct cases, experimental perturbation functions measured at temperatures below and above T_C. At temperatures above T_C, the perturbation functions for stoichiometric samples of $ZrFe_2$ show very weak nuclear electric-quadrupole interactions (NQI's) that represent broad distributions of EFG's and, correspondingly, interaction frequencies. The aforementioned model of an NQI does not provide a unique set of parameters that gives an accurate representation of the experimental measurement. Instead, adequate representations could be achieved by assuming one, two, or several distinct interaction sites. For the nonstoichiometric samples, the above-T_C perturbation functions show stronger NQI's than those for the stoichiometric samples, and these perturbation functions also represent broad distributions of interaction frequencies. To achieve an accurate representation of these perturbation functions requires assuming at least two interaction sites.

At temperatures well below T_C, the perturbation functions show two components. Each of these components corresponds to a strong magnetic-dipole interaction perturbed by a weak electric-quadrupole interaction. Generally, for the stoichiometric samples, one of the two combined interactions dominates, representing 70–80% of the probes. The other, higher-frequency interaction represents the remainder of the probes. To represent these perturbation functions accurately requires using the (aforementioned) model of combined magnetic and quadrupole interactions. At temperatures very

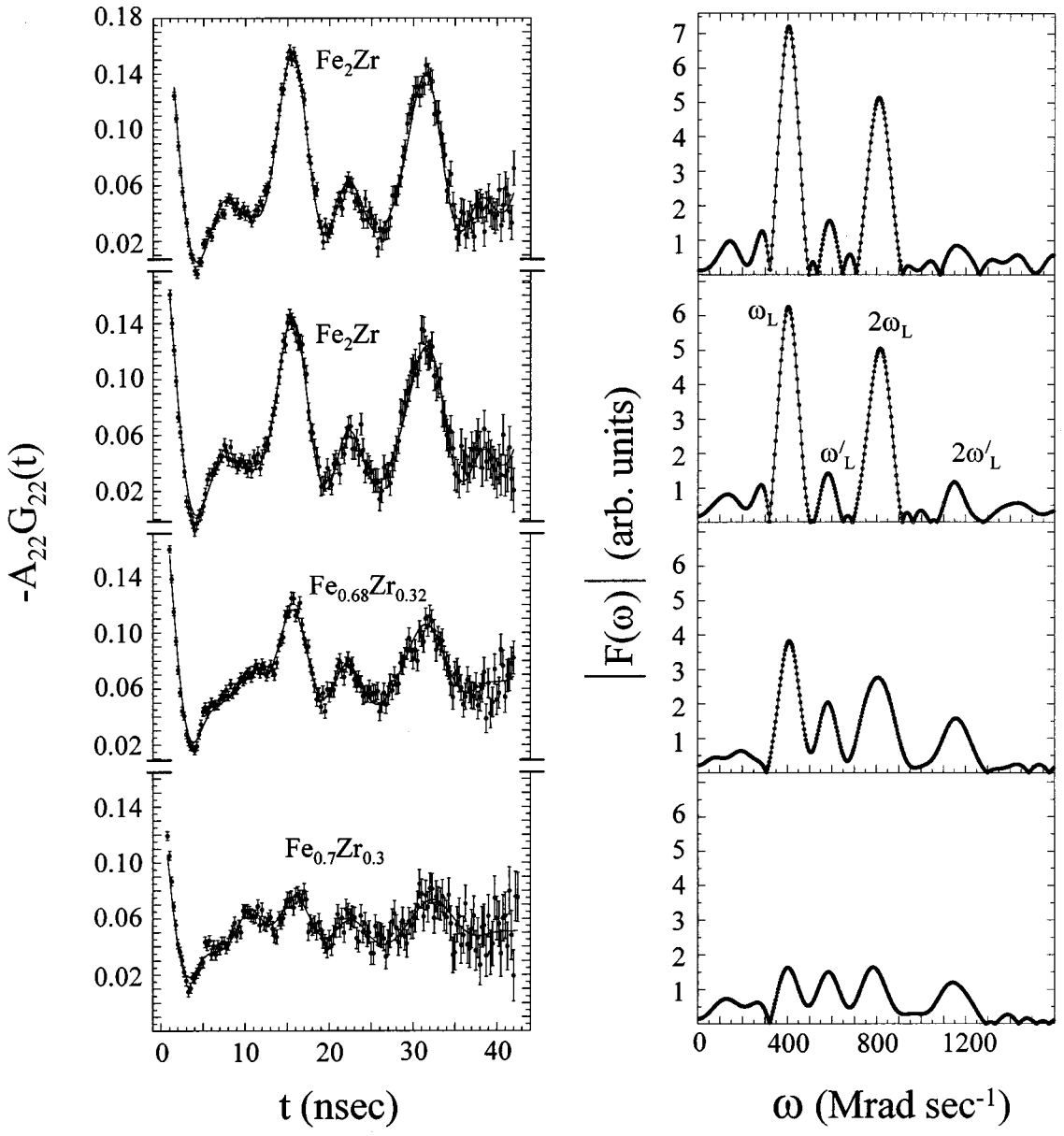

FIG. 3. Perturbation functions and corresponding Fourier transforms, measured at laboratory temperature on (1) a stoichiometric sample of $ZrFe_2$ (top and second-from-top figures), (2) an Fe-rich sample having composition $Zr_{0.32}Fe_{0.68}$ (third-from-top figure), and (3) an Fe-rich sample having composition $Zr_{0.30}Fe_{0.70}$ (bottom figure), show line broadening that increases as the Fe concentration increases.

near but below T_C, the effects of the two magnetic-dipole interactions cannot be separated, because the corresponding interaction frequencies approach each other in magnitude. In addition, the distributions associated with these frequencies become broader and comparable in magnitude to the frequencies that arise from the NQI.

IV. RESULTS

Figure 2 presents perturbation functions and corresponding Fourier transforms for a stoichiometric sample ($y=0$) of $(Zr_{1-x},Hf_x)\ Fe_{2+y}$ measured at temperatures ranging from laboratory temperature to just below T_C. In the Fourier transforms, the two magnetic-dipole interactions, characterized by the frequencies ω_L and $2\omega_L$, are clearly evident. The peak amplitudes in the transforms reflect the relative fraction of the probes that undergo the corresponding interaction. For a pure magnetic-dipole interaction in a polycrystalline sample, the amplitudes of the two components for frequencies ω_L and $2\omega_L$ should be equal. Thus the broadening of the peaks indicates the effect of the weak, poorly-defined NQI, which is operative over the entire investigated temperature range. At temperatures approaching T_C, the peaks in the Fourier transforms become difficult to resolve. At laboratory temperature (290 K), we consistently obtained $\omega_L=407(1)$ Mrad sec^{-1} and $\omega_L=579(3)$ Mrad sec^{-1}, and the ratio of these two values is 1.42(1), which corresponds to magnetic hyperfine fields of 93.0(0.5) kOe and 65.4(0.2) kOe. These values correspond quite well to the ratio of 1.413 and values of the hyperfine field 92 and 62.5 kOe obtained by Livi, Amaral, and Fries[11] on similar samples.

In Fig. 3 we present several laboratory-temperature perturbation functions and corresponding Fourier transforms that show the effects produced by changing the Fe composi-

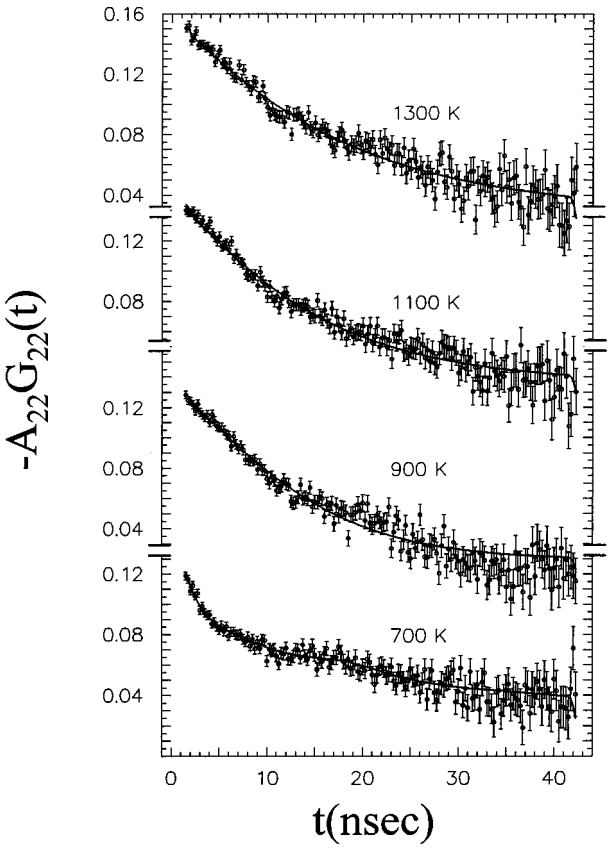

FIG. 4. Perturbation functions, which were measured at a series of elevated temperatures on an Fe-rich sample having composition $Zr_{0.30}Fe_{0.70}$, show more line broadening than in the corresponding case of stoichiometric samples, which Fig. 3 shows. The fits to the measured functions represent a model of two NQI's, which broad distributions of frequencies characterize.

tion. The top perturbation function represents a measurement performed on a stoichiometric sample of $ZrFe_2$. The next two measurements correspond to a single stoichiometric sample of $ZrFe_2$ that we divided into two pieces. We remelted one piece without addition of Fe, and we remelted the other piece with enough extra Fe to increase its composition from 66.66–68 at. % Fe. The measurement shown in the bottom of Fig. 3 corresponds to a sample prepared with the composition $Zr_{0.3}Fe_{0.7}$. Together, these perturbation functions and Fourier transforms show that an increase in Fe concentration from the stoichiometric value gives rise to increased line broadening and an increased fraction of probes that undergo the secondary higher-frequency magnetic-dipole interaction.

The perturbation functions for a Fe-rich sample with composition $Zr_{0.3}Fe_{0.7}$ measured at several elevated temperatures appear in Fig. 4. The functions show two components—a higher-frequency component that dominates the earlier-time regions and a lower-frequency component that dominates the later-time regions of the perturbation functions. This observation suggests that excess Fe and the origin of the secondary interaction are correlated. To represent the measured perturbation functions, a model that includes two NQI's and a model that consists of two exponential-decay terms work equally well. The former represents the effects of static EFG's, which, presumably in this case, randomly located defects generate. The latter represents the effects of fluctuating EFG's. Unfortunately, the effects of prompt coincidences obscure the information in the perturbation functions at times less than two or three nanoseconds. In principle, this information could be used to determine which of these two models gives a more accurate physical representation, because the curvature of $G_{22}(t)$ for small values of t differs for the two models. Moreover, if fluctuating EFG's were operative, their fluctuation rates would be insufficiently fast, in order to reduce the anisotropy to zero within the experimental time scale of $\approx$40 nsec. Hence distinguishing between static and time-varying EFG's in this case is problematical.

Figure 5 presents perturbation functions for a stoichiometric sample of $ZrFe_2$ measured at a series of temperatures very close to T_C and at two temperatures above T_C (633.0 and 1300 K). The two perturbation functions measured at a temperature very close to but above T_C and a temperature well above T_C show no discernible temperature dependence, which is consistent with the source of the interaction being immobile point defects. These two perturbation functions are representative of many that we measured at temperatures above T_C. This series of measurements performed below T_C shows the gradual evolution of the interaction frequencies and line shapes, which characterizes the ferromagnetic-to-paramagnetic transition. As the temperature increases, the frequencies decrease in magnitude and the line shapes broaden, which, for temperatures within $\approx$20 K of T_C, makes the separation of the components indeterminate. Likewise, we are unable to determine the power-law dependence of ω_L on reduced temperature $[\omega_L = \omega_L(0)t_r^{\beta}, \ t_r = 1 - (T/T_C)]$ at temperatures very close to T_C (however, from about 500–600 K both MHF's show a power-law exponent $\beta = 0.3$).

We can, however, estimate T_C by visual inspection. The perturbation function measured at 633 K shows the evolution to the high-temperature shape, which remains invariant over several hundred degrees, whereas, the function measured at 629 K shows qualitatively a stronger perturbation. Therefore T_C must lie between these two temperatures, $T_C = 631(2)$ K. Figure 6 presents the temperature dependence of the Larmor frequencies for the two MHF's. The temperature dependence of the primary interaction confirms the determination of T_C. In one series of measurements, the temperature was increased in successive steps; and in another series, temperature was decreased successively. We cannot resolve differences in the temperature dependence of the frequencies that represent the two series. Therefore we observe no hysteresis, within the experimental accuracy.

V. DISCUSSION

As discussed above, based on the crystal structure and on the local symmetry at the Zr site in the $ZrFe_2$, we would expect to observe no nuclear electric-quadrupole interaction at the Zr site. Above the magnetic ordering temperature T_C, we would expect the γ-γ angular correlation to show no perturbations; and, below T_C, in the γ-γ angular correlation, we would expect to observe a single well-defined magnetic-dipole interaction. However, both the results of this work and the previous work of other researchers[11] show that weak EFG's and two MHF's characterize the hyperfine interactions at the Zr site in $ZrFe_2$ below T_C.

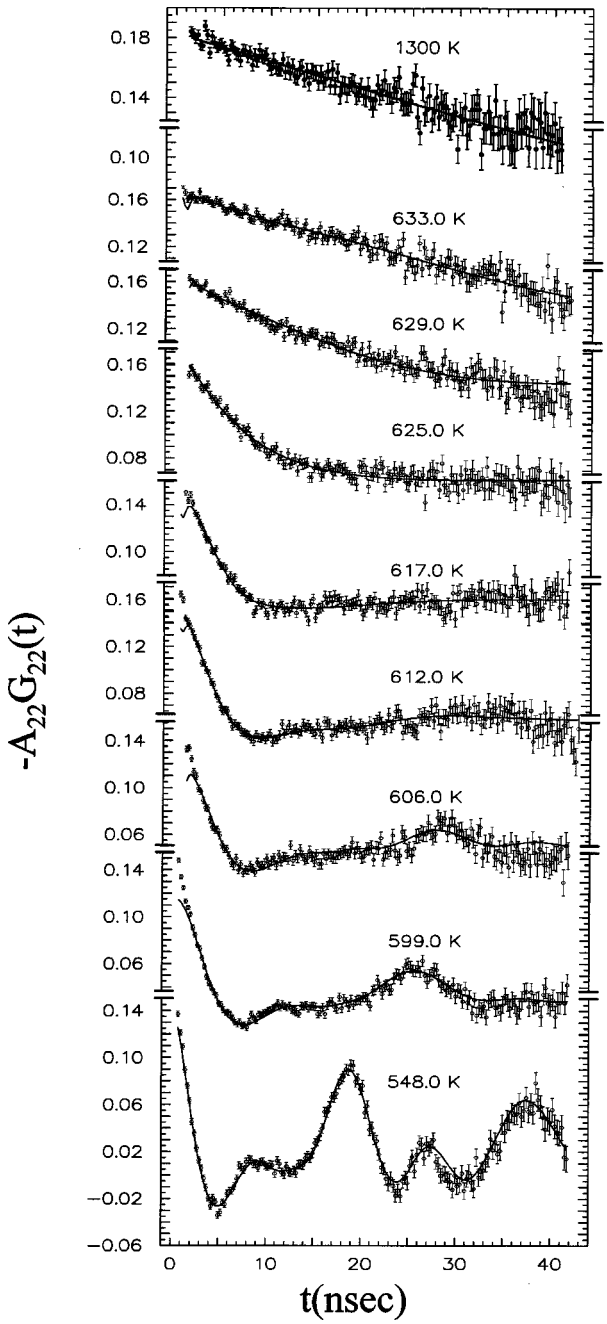

FIG. 5. The top two perturbation functions were measured at approximately 700 K above T_C and at just one or two degrees above T_C. These functions show clearly that the NQI has no temperature dependence in the range of interest. (The difference in the anisotropy between these two perturbation functions arises from instrumental effects.) The other perturbation functions measured below T_C illustrate the changes in the combined interaction that arise as the temperature approaches T_C. At temperatures very close to but below T_C, the first 5–10 nanoseconds of the perturbation function represent the frequency information. The fits in this region represent the average effect of the weak NQI combined with the two magnetic-dipole interactions. This feature does not allow us to resolve the individual ω_L values in this region.

To explain these observations, we consider the fractions of probes corresponding to the two magnetic-dipole interactions, which are 70–80% for the lower-frequency interaction (majority interaction) and approximately 20–30% for the higher-frequency interaction (minority interaction). (We made several samples of $ZrFe_2$, and observed that these site fractions fluctuated about the aforementioned values by about 5%.) At a Zr site in $ZrFe_2$, a Zr atom has four Zr-atom next-nearest neighbors. If some type of point defect were present in relatively high concentrations of a few percent and randomly distributed in the crystal, then the probability that, at a given Zr atom, a point defect is located in either coordination sphere would be approximately 0.2–0.3. Therefore the observed probe site fractions, which correspond to the two magnetic-dipole interactions, are consistent with the hypothesis that the origin of the frequency increase in the interaction corresponding to the ≈20% fraction is a point defect and that concomitantly the origin of the ≈80% fraction is a defect-free ''perfect-crystal'' probe environment.

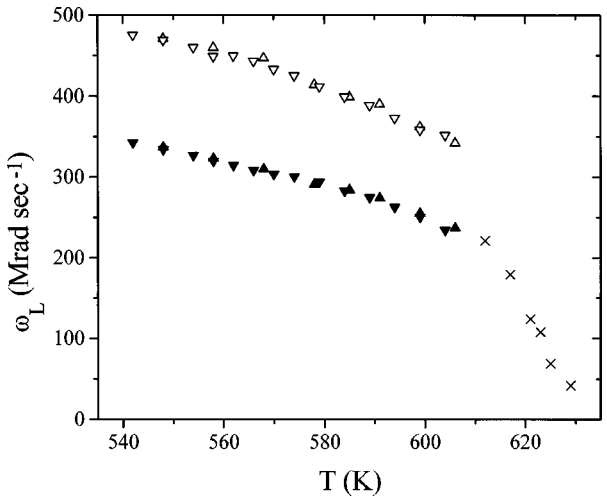

FIG. 6. Temperature dependence of the two magnetic-dipole interactions. The solid triangles represent the majority interaction, which represents approximately 80% of the probes. The open triangles represent the minority interaction, which represents approximately 20% of the probes. The experimental points, which were obtained as part of a series where the temperature increased, are shown in right-side-up triangles, while those obtained in series where the temperature decreased are shown as inverted triangles. The uncertainties for these values are smaller than the size of the data points. The crosses represent frequency values that correspond to the average effect of the weak NQI combined with two very weak magnetic-dipole dipole interactions. Because these points represent phenomenological nonphysical fits primarily to the early-time regions of the perturbation functions, we cannot assign physically meaningful uncertainties to them. However, we can estimate $T_C = 631(2)$ K, using a line drawn through the crosses and the inspection of Fig. 5.

We consider further the hypothesis that primarily a single type of point defect causes the minority higher-frequency magnetic-dipole interaction. Although this hypothesis implies a relatively high defect concentration. Muraoka, Shiga, and Nakamura,[9] Yamada and Ohira,[21] and Wiesinger, Oppelt, and Buschow[10] observed that Fe antisite defects, i.e., Fe atoms that reside on Zr sites, arise commonly even for stoichiometric samples in the $ZrFe_2$ crystal. Additionally, probe-defect interactions could cause the distribution of defects to be not completely random. This effect would lead to a higher minority interaction site occupancy at lower global defect concentrations.

In addition to changing the observed MHF below T_C, the

antisite defects are also likely to contribute to the NQI. This is because the lattice distortion associated with the antisite defect breaks the cubic symmetry around the Zr site. The resulting NQI, combined with those caused by other defects that might be present in the compound can lead to the observed quadrupole interaction above and below T_C.

Moreover, as Fig. 3 indicates, the site fraction for the minority interaction (high-frequency MHF) increases as the concentration of excess Fe increases. The associated line broadening, which also increases with the excess Fe concentration, corresponds to changes in the magnetic hyperfine interactions from the existence of different types of defects at higher concentrations. Measurements, which we performed above T_C on the Fe-rich sample and which Fig. 4 shows, also indicate that the addition of excess Fe gives rise to a stronger NQI, which a broad distribution of frequencies characterizes. An increased concentration of defects associated with the departure from stoichiometry could cause this stronger NQI. The line broadening could be caused by the existence of different types of different NQI's that accompany higher defect concentrations.

To test this hypothesis further, we asked Legoas and coworkers to calculate MHF's and the corresponding Larmor frequencies ω_L at the Zr site for several types of defects in the $ZrFe_2$ structure. They used the real-space, linear muffin-tin orbital atomic sphere approximation (RS-LMTO-ASA) method.[22,23,24] They performed these calculations for a Ta atom at a Zr site for four different situations: (1) a perfect crystal, (2) an antisite defect Fe→Zr in a nearest-neighbor Zr site, (3) a vacancy in a nearest-neighbor Fe site, and (4) a vacancy in a nearest-neighbor Zr site. The ratio of the value of the hyperfine field with the corresponding defect present, cases 2, 3, and 4, and the value of the perfect-crystal hyperfine field, case 1, yield: 1.8 for case 2, the antisite defect Fe in a nearest-neighbor Zr site; 1.5 for case 3, a nearest-neighbor Fe vacancy; and 2.6 for case 4, a nearest-neighbor Zr vacancy. The measured ratio of the higher-frequency (minority) MHF to the lower-frequency (majority) MHF is 1.42. The ratios for cases 2 and 3 are sufficiently close to the experimental ratio, given the uncertainties in the calculations and the experiments, that we cannot rule out either possibility. However, we can rule out case 4, a vacancy in a nearest-neighbor Zr site, because the calculated ratio of 2.6 deviates sufficiently from the experimental ratio of 1.42. Therefore to identify the origin of the minority MHF, these model calculations do not uniquely allow us to distinguish between the Fe antisite defect and the nearest-neighbor Fe-site vacancy.

According to the model calculations, the observed probe site fractions, corresponding to the two magnetic-dipole interactions, are consistent with the hypothesis that the difference (from the majority interaction) in the interaction magnitude corresponding to minority interaction arises from an Fe antisite point defect and that concomitantly the origin of the majority interaction is a ''perfect-crystal'' probe environment. We base this conclusion on (1) the correlation between excess Fe concentration and the minority site fraction, (2) the line shapes corresponding to the NQI's and the related broadening of the lines corresponding to the magnetic-dipole interactions, and (3) empirical evidence obtained from other measurements for Fe antisite defects in $ZrFe_2$.

Additionally, from sample to sample, we varied the Hf concentration in $(Zr_{1-x},Hf_x)\ Fe_{2+y}$ from $x=0.003-0.04$, and we observed no strong dependence of these site fractions on this concentration. Therefore the point defect in question is not related to the Hf doping and is an indigenous defect. Moreover, we observe only two well-defined MHF's. We assign the majority interaction to a near ''perfect-crystal'' environment located in the vicinity of the probe atoms. The minority interaction, we ascribe to the alteration of the transferred spin density produced by an Fe atom that lies on a nearest-neighbor Zr site. We observe no other magnetic-dipole interactions. Therefore we conclude that the defects, which provide stoichiometric compensation for the envisioned Fe antisite defects, are not localized with respect to the probe atoms. The accommodation of the stoichiometry variation could occur through extended defects, such as antiphase boundaries, or through the existence of small amounts of an undetected Zr-rich second phase. The reproducibility and consistency of measurements performed on a variety of samples suggests strongly that perfect order does not characterize the thermodynamically stable crystal structure. Instead the stable structure crystallizes with a small amount of disorder.

VI. CONCLUSIONS

We have measured the temperature dependence of a primary MHF, a secondary MHF, and a weak EFG at the Zr-site in several samples of $ZrFe_2$. Using experimental and theoretical information, we have identified the sources of the two MHF's. The primary, lower-frequency MHF represents a nearly ''perfect-crystal'' Zr-site probe environment, in which the transfer of spin density from Fe *d* orbitals polarizes the ^{181}Ta nuclei. The secondary, higher-frequency MHF represents a probe environment in which a nearest-neighbor Fe antisite defect in a Zr site augments the transferred hyperfine field. Calculations of the MHF's performed using the RS-LMTO-ASA method are consistent with this interpretation. At temperatures very close to but below T_C, the frequencies corresponding to the two Zr-site MHF's approach each other in value. For this reason, we cannot resolve the power-law dependence of either MHF at temperatures very close to T_C.

ACKNOWLEDGMENTS

We are greatly indebted to S. B. Legoas and S. Frota-Pessôa of the University of São Paulo, Brazil, for performing the *ab initio* calculations of MHF's in $ZrFe_2$. We would like to thank Jim Garrett of McMaster University for providing initial samples of $ZrFe_2$ and Ron Eaken of the Radiation Science and Engineering Center (RSEC) at Penn State for building the arc-melting apparatus. We gratefully acknowledge the RSEC for producing the ^{181}Hf isotope. One of us (R.L.R.) gratefully acknowledges the hospitality of the Fakultät für Physik at the University of Konstanz where part of this work was performed. We greatly appreciate support from the National Science Foundation from Grant No. INT-9503934 and support from the Brazilian National Research Council (CNPq).

[1] G. L. Catchen, MRS Bull. **20**, 37 (1995).
[2] H. J. Wallbaum, Z. Kristallogr. **103**, 391 (1941).
[3] D. Arias and J. P. Abriata, Bull. Alloy Phase Diagrams **9**, 597 (1988).
[4] F. Aubertin, U. Gonser, S. J. Campbell, and H.-G. Wagner, Z. Metallkd. **76**, 237 (1985).
[5] G. K. Wertheim, V. Jaccarino, and J. H. Wernick, Phys. Rev. **135**, A151 (1964).
[6] L. Amaral, F. P. Livi, and A. A. Gomes, J. Phys. F **12**, 2091 (1982).
[7] E. Piegger and R. S. Craig, J. Chem. Phys. **39**, 137 (1963).
[8] W. Bruckner, K. Kleinstuck, and G. E. R. Schulze, Phys. Status Solidi **23**, 475 (1967).
[9] Y. Muraoka, M. Shiga, and Y. Nakamura, J. Phys. F **9**, 1889 (1979).
[10] G. Wiesinger, A. Oppelt, and K. H. J. Buschow, J. Magn. Magn. Mater. **22**, 227 (1981).
[11] F. P. Livi, L. Amaral, and S. G. Fries, Phys. Status Solidi A **53**, 379 (1979).
[12] V. Sevchovsky, G. Wiesinger, and J. Toul, Physica B & C **B102**, 212 (1980).
[13] H. Betsuyaki and S. Komura, J. Phys. Soc. Jpn. **19**, 1262 (1964).
[14] P. Mohn and K. Schwarz, Physica B & C **130B**, 26 (1985).
[15] T. Dumelow, P. C. Riedi, P. Mohn, K. Schwarz, and Y. Yamada, J. Magn. Magn. Mater. **54-57**, 1081 (1986).
[16] J. G. M. Armitage, T. Dumelow, R. H. Mitchell, P. C. Riedi, J. S. Abell, P. Mohn, and K. Schwarz, J. Phys. F **16**, L141 (1986).
[17] R. Luck and H. Wang, J. Alloys Compd. **191**, L11 (1993).
[18] S. Komura and N. Shikazono, J. Phys. Soc. Jpn. **18**, 323 (1963).
[19] G. Schatz and A. Weidinger, *Nuclear Condensed Matter Physics: Nuclear Methods and Applications*, 2nd ed. (Wiley, New York, 1996).
[20] B. Lindgren, Hyperfine Interact. **C1**, 613 (1996).
[21] Y. Yamada and K. Ohira, J. Phys. Soc. Jpn. **52**, 3646 (1983).
[22] P. R. Reduto, S. Frota-Pessôa, and M. S. Methfessel, Phys. Rev. B **44**, 13 283 (1991).
[23] S. B. Legoas and S. Frota-Pessôa (unpublished).
[24] S. B. Legoas, Ph.D. thesis, 1998, University of Sao Paulo, Brazil.